electronics

MDPI

Article

Improving Electric Vehicle Structural-Borne Noise Based on Convolutional Neural Network-Support Vector Regression

Xiaoli Jia [1], Lin Zhou [2,*], Haibo Huang [3], Jian Pang [1] and Liang Yang [1]

[1] State Key Laboratory of Vehicle NVH and Safety Technology, Chongqing Chang'an Automobile Co., Ltd., Chongqing 401133, China; jiaxl@changan.com.cn (X.J.); pangjian@changan.com.cn (J.P.); yangliang2@changan.com.cn (L.Y.)
[2] Chongqing Metropolitan College of Science and Technology, Chongqing 401320, China
[3] School of Mechanical Engineering, Southwest Jiaotong University, Chengdu 610031, China; huanghaibo214@swjtu.edu.cn
* Correspondence: zhoulin@cqcst.edu.cn

Abstract: In order to enhance the predictive accuracy and control capabilities pertaining to low- and medium-frequency road noise in automotive contexts, this study introduces a methodology for Structural-borne Road Noise (SRN) prediction and optimization. This approach relies on a multi-level target decomposition and a hybrid model combining Convolutional Neural Network (CNN) and Support Vector Regression (SVR). Initially, a multi-level target analysis method is proposed, grounded in the hierarchical decomposition of vehicle road noise along the chassis parts, delineated layer by layer, in accordance with the vibration transmission path. Subsequently, the CNN–SVR hybrid model, predicated on the multi-level target framework, is proposed. Notably, the hybrid model exhibits a superior predictive accuracy exceeding 0.97, surpassing both traditional CNN and SVR models. Finally, the method and model are deployed for sensitivity analysis of chassis parameters in relation to road noise, as well as for the prediction and optimization analysis of SRN in vehicles. The outcomes underscore the high sensitivity of parameters such as the dynamic stiffness of the rear axle bushing and the large front swing arm bushing influencing SRN. The optimization results, facilitated by the CNN–SVR hybrid model, align closely with the measured outcomes, displaying a negligible relative error of 0.82%. Furthermore, the measured results indicate a noteworthy enhancement of 4.07% in the driver's right-ear Sound Pressure Level (SPL) following the proposed improvements compared to the original state.

Keywords: structural-borne road noise; multi-level target decomposition; CNN–SVR hybrid model; optimal design

check for updates

Citation: Jia, X.; Zhou, L.; Huang, H.; Pang, J.; Yang, L. Improving Electric Vehicle Structural-Borne Noise Based on Convolutional Neural Network-Support Vector Regression. *Electronics* **2024**, *13*, 113. https://doi.org/10.3390/electronics13010113

Academic Editor: Hamid Reza Karimi

Received: 26 November 2023
Revised: 17 December 2023
Accepted: 26 December 2023
Published: 27 December 2023

Copyright: © 2023 by the authors. Licensee MDPI, Basel, Switzerland. This article is an open access article distributed under the terms and conditions of the Creative Commons Attribution (CC BY) license (https://creativecommons.org/licenses/by/4.0/).

1. Introduction

As the automobile industry enters a period of steady growth with connotative development, automobile quality improvement becomes the mainstream of development. This necessitates an intensified focus on Noise, Vibration, and Harshness (NVH) in automobiles, where NVH performance assumes a pivotal role as a critical metric for gauging overall automotive quality [1]. New energy vehicles, marked by their emphasis on environmental sustainability and energy conservation, confront distinctive challenges [2]. Notably, the absence of the masking effect associated with traditional engine noise accentuates the prominence of other sources of noise, including road noise, motor noise, and fan noise [3,4]. Among these, road noise emerges as the predominant contributor to the comprehensive acoustic profile of a vehicle, commanding heightened attention.

Road noise, contingent upon its transmission path, delineates into air-borne noise and structural-borne noise [5]. Air-borne noise predominantly spans the middle- to high-frequency spectrum, ranging from 300 Hz to 8000 Hz, emanating primarily from the tires and the noise generated by road friction. Addressing air-borne noise involves strategic

interventions such as acoustic packaging and the optimal design of tires [6]. In contrast, structural-borne noise predominates in the frequency band from 20 Hz to 300 Hz, manifesting as noise transmitted through structural pathways. Frequently characterized by driver and passenger complaints of "low-frequency drumming" and "mid-frequency rumbling", Structural-borne Road Noise (SRN) assumes particular significance [7,8]. The transmission path of structural-borne noise is intricate and challenging to control, but it is very easy to cause discomfort to drivers and passengers, which is the focus of this paper.

The prevailing methodologies for road noise analysis predominantly encompass real-vehicle testing and Computer-Aided Engineering (CAE) simulation. Gao Yu et al. [9] demonstrated the optimization of tire cavity noise by leveraging real-vehicle test data and a transfer path analysis model, resulting in effective suppression of interior noise. Likewise, Yu Xiongying et al. [10], employing real-vehicle tests and transmission path theory, successfully identified the principal transmission path of road noise. The vehicle's road noise issue is effectively resolved with the rear axle construction modification. While the efficacy of test-based approaches in mitigating road noise is evident, challenges such as prolonged test cycles, unpredictability in the initial stages, difficulty in subsequent rectification, and elevated costs underscore the need for alternative strategies. To address these challenges and enable proactive prediction of road noise, CAE simulation methods are gaining prominence, based on which the vehicle structure or parameters can be optimized, and according to the optimization results, the optimal solution is provided to guide the test, so as to achieve the reduction of vehicle interior noise. Kido et al. [11] established a comprehensive finite element model of the entire vehicle, encompassing tires, suspension, and the body system. This model predicted the road noise below 120 Hz. Similarly, Chen Shuming et al. [12] applied excitation forces from a real vehicle road test to a body acoustic-structural coupling model, predicting interior noise within the range of 20 Hz to 200 Hz. Despite the growing adoption of CAE simulation methods for road noise analysis, challenges persist due to the myriad influencing factors, intricate formation mechanisms, and pronounced nonlinearity associated with road noise. Limitations such as difficulty in acquiring certain parameters, challenges in expressing the nonlinear behavior of elastic elements, and protracted cycle times for refined model modeling and computation impede the comprehensive support for the pre-development of automotive road noise performance through finite element models established via CAE simulation methods. The swift progression of artificial intelligence technology has engendered notable advancements in NVH research, particularly through the application of machine learning methods. Xing Y.F et al. [13] constructed a model grounded in artificial neural network methods, effectively predicting interior noise sound quality. Additionally, Liang Linyuan et al. [14] evaluated vehicle interior impact noise induced by speed bumps based on support vector machine methods, and they achieved accurate forecast results. These research findings serve as valuable references for researchers contemplating road noise analysis through machine learning methodologies [15]. Nonetheless, extant challenges necessitate innovative approaches. A primary challenge emanates from the intricate interplay among the road surface, tires, suspension, body, and other systems inherent in road noise generation. Owing to the multitude of influencing factors and complex transmission paths [16], the direct construction of an approximation model for underlying parameters and vehicle interior noise bears the risk of underfitting. Such an approach is counterproductive to the precise identification of principal transmission paths and the rectification of road noise-related issues. A secondary challenge arises from the complex formation mechanism and pronounced nonlinearity characterizing road noise. Traditional shallow networks exhibit limited efficacy in addressing such intricate problems [17]. Given that the prediction and optimization of road noise are significantly impacted by the approximation model's accuracy, it is imperative to enhance the fitting accuracy of the approximation model to secure precise prediction results in road noise analysis. To solve the previously listed issues, this study presents a multi-level target decomposition method and a Convolutional Neural Network–Support Vector Regression (CNN–SVR)

hybrid model, which is applied to improve the prediction accuracy and control capability of low- and medium-frequency road noise in automobiles.

Two major contributions are made by this study: (1) A multi-level target decomposition method is proposed based on the hierarchical decomposition of vehicle road noise along the chassis components, defined layer by layer in accordance with the vibration transmission path. Consequently, the prediction and optimization of road noise are no longer limited to the top-level road noise performance and the bottom-level component parameters, but rather, they are used to match and analyze the performance of the sub-systems hidden between the systems. (2) On this basis, given the powerful feature extraction capability of CNN and the advantages of the SVR algorithm in small-sample scenarios, an SRN prediction model combining CNN and SVR algorithm is established to improve its accuracy. Based on the proposed multi-level decomposition method and CNN–SVR hybrid model, the improved vehicle is treated to carry out SRN prediction and optimization design, and the measured outcomes validate the efficacy of the suggested approach.

This is how the rest of the paper is structured. The multi-level target decomposition technique and CNN–SVR hybrid model are introduced in Section 2. The SRN prediction model is created in Section 3, and its accuracy is contrasted with that of the conventional CNN and SVR models. In Section 4, the road noise is improved by the suggested approach, and the effect is verified in the actual vehicle. Section 5 provides a summary of the paper's findings.

2. Research Methods

2.1. Multi-Level Target Decomposition Method for SRN

SRN is generally stimulated by roads, tires through the front and rear suspension system connecting rods, and elastic components transferred to the body, causing the body wall plate vibration and radiation noise to the interior of the vehicle and ultimately transferred to the human ear. Figure 1 depicts the SRN transmission process from the perspective of the "source-path-receiver".

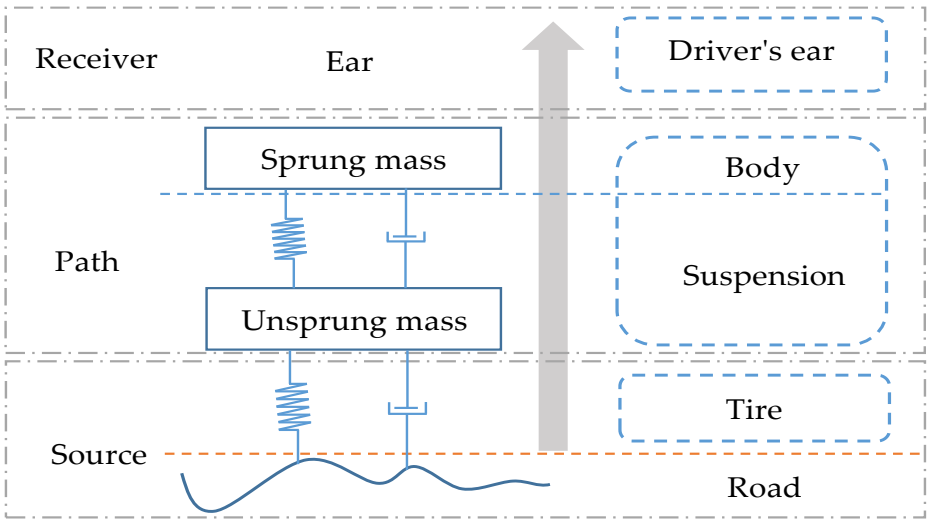


Figure 1. SRN transmission process.

In this paper, the vehicle with front MacPherson suspension and rear torsion beam suspension is studied to analyze its SRN transmission path. The front MacPherson suspension consists of the swing arm, shock absorber, and coil spring, and the rear torsion beam suspension consists of the rear axle, shock absorber, and coil spring. The SRN transmission path in Figure 2, shows that the unilateral front MacPherson suspension contains three transmission paths, the unilateral rear torsion beam suspension contains three transmission paths, and the unilateral front and rear suspensions contain a total of six transmission paths. In vehicle systems, the elastic elements that attenuate vibration transmission are

the key factors affecting road noise. The matching of parameters between systems is the fundamental cause of the road noise issue. Parameters that have a significant impact on road noise include tire stiffness and damping parameters, dynamic stiffness parameters of the highly sensitive bushing of the suspension, and damping force parameters of the shock absorber. The parameters that have less influence on road noise include coil spring stiffness parameters and low-sensitive bushing stiffness parameters [18]. Among them, although the tire stiffness and damping parameters have a greater impact on road noise, the acquisition and rectification of its parameters are more difficult, so this paper introduces knuckle excitation instead of tire and road excitation, temporarily avoiding tire study, thus reducing the complexity of the prediction model. In this work, the road and tires are used as control variables, focusing on the effect of chassis elastic element parameters on road noise. Tire selection of radial tires, tire specifications for 225/55 R18, tire pressure is set to 2.5 bar.

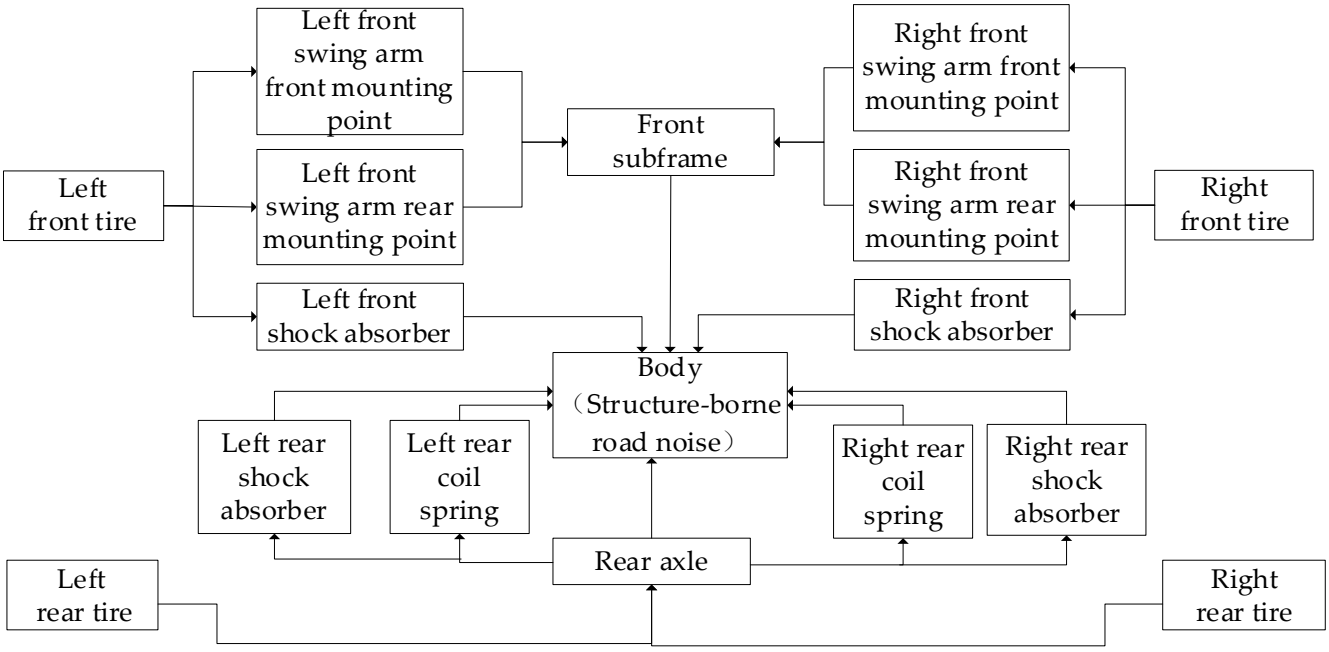


Figure 2. SRN transmission path.

According to the SRN transmission relationship, the road noise along the vibration transmission path is decomposed layer by layer to the chassis component parameters. Accordingly, the SRN multi-level decomposition architecture is established, as shown in Figure 3. Among them, the top-level design target is the driver's right-ear Sound Pressure Level (SPL); the adjacent lower-level design variables are the passive side vibration response of the suspension and body attachment points (including front subframe front mounting point, front subframe rear mounting point, front shock absorber upper mounting point, rear axle mounting point, rear coil spring mounting point, and rear shock absorber upper mounting point); further downward decomposition of the adjacent lower-level design variables are the active side vibration response at the suspension-body attachment points (including front swing arm front mounting point, front swing arm rear mounting point, and rear axle mounting point) and the dynamic parameters of the suspension components (including dynamic stiffness of the front swing arm front and rear bushings, dynamic stiffness of the front and rear shock absorber upper mounting bushings, front and rear shock absorber damping force, front and rear coil spring stiffness, dynamic stiffness of the rear axle bushing); and the bottom level is the vibration excitation from knuckle, and the ball-hinge bushing dynamic parameters. The decomposition principle of the road noise multi-level decomposition architecture is that the design goals of the upper level

are decomposed downward into the excitation of the nearby lower level and the dynamic parameters of the connecting elements.

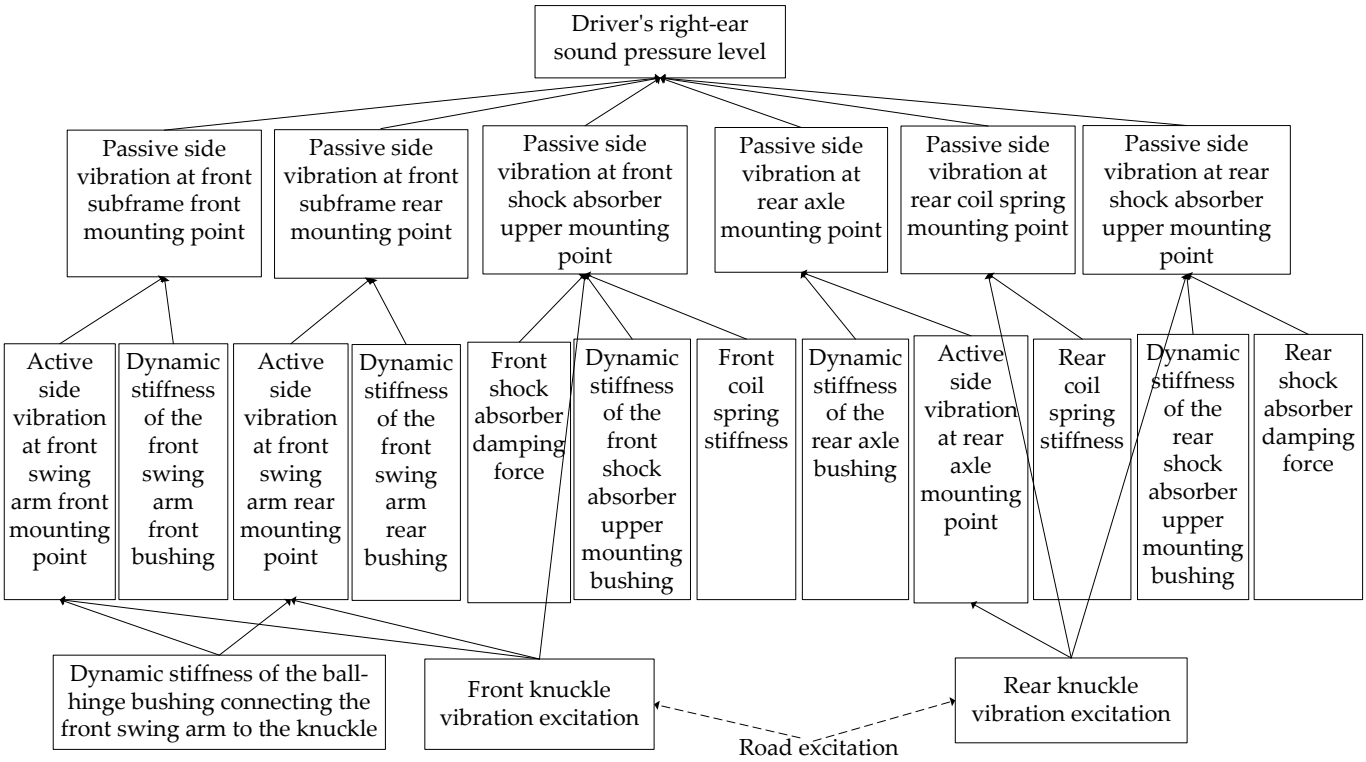


Figure 3. Road noise multi-level decomposition architecture.

2.2. Proposed CNN–SVR Prediction Method

It is challenging to forecast road noise because it incorporates several systems, a wide range of influencing elements, intricate production mechanisms and transmission pathways, and substantial nonlinearity. The existing simulation-based prediction techniques suffer from low accuracy and efficiency [19], and developing a comprehensive mechanistic model is extremely challenging. This research presents a data-driven approach to road noise prediction in an effort to increase prediction efficiency and accuracy. Given that deep networks need a high sample size, standard shallow networks are restricted in their capacity to suit complicated situations and extract features. This paper combines the powerful adaptive feature extraction ability of CNN and the advantages of the SVR algorithm in small data sample scenarios, then establishes a CNN–SVR hybrid model for SRN prediction. Among them, CNN, as a representative algorithm of deep learning, has excellent performance in the fields of image recognition [20–22], speech recognition [23], and target detection [24–27]. It establishes the mapping relationship between input and output through multidimensional nonlinear feature extraction, has extremely strong data characterization and mapping ability [28,29], and can obtain higher accuracy and robustness compared with traditional shallow artificial neural networks [30]. SVR is a machine learning technique founded on the concepts of structural risk minimization. [31], which can effectively solve the problems of nonlinearity, small samples, dimensional catastrophe, and local minima [32]. Combining the SVR algorithm with the CNN, which is suitable for large data samples, can achieve good results in small data sample scenarios [33]. Figure 4 displays the structure of the CNN–SVR hybrid model.

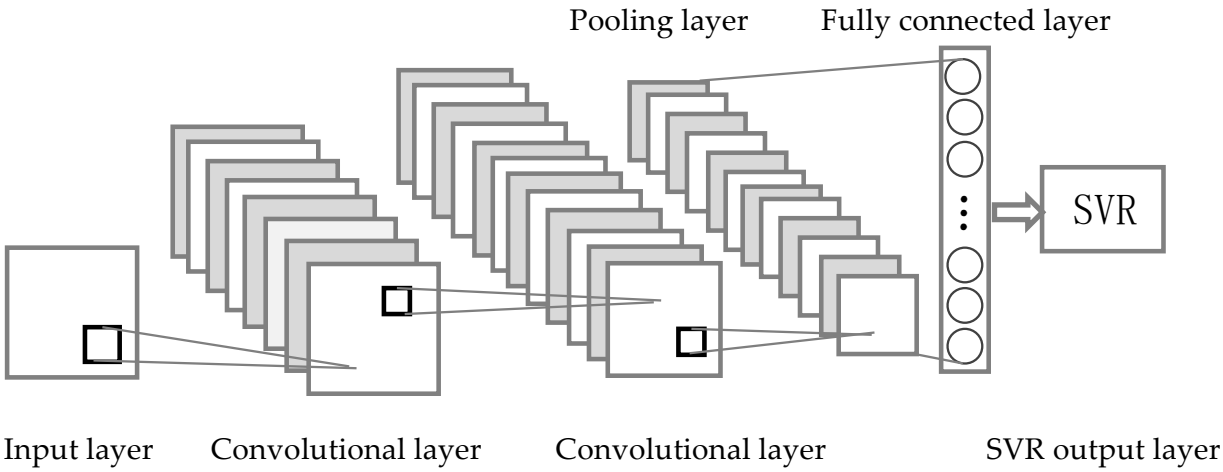


Figure 4. The structure of the CNN–SVR hybrid model.

The CNN–SVR hybrid model includes an input layer, two convolutional layers, a pooling layer, a fully connected layer, and an SVR output layer. The input layer is used to accept data input and perform data preprocessing. The convolutional layer is mostly utilized for automatic data feature extraction through the convolutional kernel. The expression of the convolution operation is shown in Equation (1) [34]:

$$\boldsymbol{X}^L = f\left(\sum_{i=1}^{L-1} \boldsymbol{k}^L * \boldsymbol{X}_i^{L-1} + \boldsymbol{b}^L\right) \tag{1}$$

where: $f(\cdot)$ represents the convolutional layer's activation function; $\boldsymbol{X}^L$ denotes the Lth convolutional layer's output matrix; $\boldsymbol{X}_i^{L-1}$ is the ith feature of the $(L-1)$th convolutional layer; $\boldsymbol{k}^L$ indicates the Lth convolutional layer's convolutional kernel; $*$ defines the convolutional operator; and $\boldsymbol{b}^L$ is the bias value.

The pooling layer comes after the convolution layer and is designed to reduce the likelihood of overfitting while increasing computational efficiency by downscaling the feature matrix that is acquired from the convolution layer. The two most popular pooling techniques are average and maximal pooling. The pooling layer's output features are enlarged into one-dimensional vectors and fed into the fully connected layer network, which is situated after the pooling layer. The fully connected layer formula is shown in Equation (2):

$$h_{w,b}(\boldsymbol{x}) = \theta(\boldsymbol{w}^{\mathrm{T}}\boldsymbol{x} + b) \tag{2}$$

where: $\theta(\cdot)$ denotes the fully connected layer's activation function; $h_{w,b}(\boldsymbol{x})$ is the output value of the neuron; $\boldsymbol{x}$ is the input feature vector of the neuron; $\boldsymbol{w}$ is the weight vector; and b is the bias.

The last layer is the SVR output layer. For the given training sample, its SVR regression function can be expressed as Equation (3) [35]:

$$y = \sum_{i=1}^{m} (\alpha_i - \alpha_i^*)\varphi(\boldsymbol{x})^{\mathrm{T}}\varphi(\boldsymbol{x}) + \beta \tag{3}$$

where: y denotes the model's predicted output value; $\boldsymbol{x}$ denotes the input feature vector; m is the number of training samples; α_i and α_i^* are the Lagrange multipliers; $\varphi(\cdot)$ is the mapping function; and β is the bias value.

The Radial Basis Function (RBF) with higher fitting accuracy is chosen as the kernel function for this paper. In order to enhance the nonlinear expression ability of the neural network model, the activation function is introduced, and the ReLU function, which is more efficient in operation, is chosen [36]. In summary, the CNN–SVR hybrid model established

in this article is based on the CNN to extract the data features, and the extracted features are used as inputs for SVR so as to predict road noise caused by structures.

Figure 5 displays a flowchart for SRN prediction based on CNN–SVR. The prediction process includes two parts: data acquisition and processing and CNN–SVR model training and validation. The detailed steps include the following: (1) Based on the road noise transmission path analysis and multi-level decomposition architecture, pre-screen the factors that have a large impact on road noise. The sample data required for constructing the road noise prediction model are collected through road experiments, and the data are preprocessed. (2) Construct the CNN–SVR hybrid model, optimize the model parameters, and train and evaluate the model based on the sample data of the training data and validation data. The process is complete if the model converges and satisfies the termination conditions (maximum epoch, predetermined accuracy requirements, etc.). If not, more sample data must be added or the model parameters adjusted until the requirements are met, and the test data is used to further assess the model's generalization capacity. Finally, the ideal parameter model for road noise is obtained.

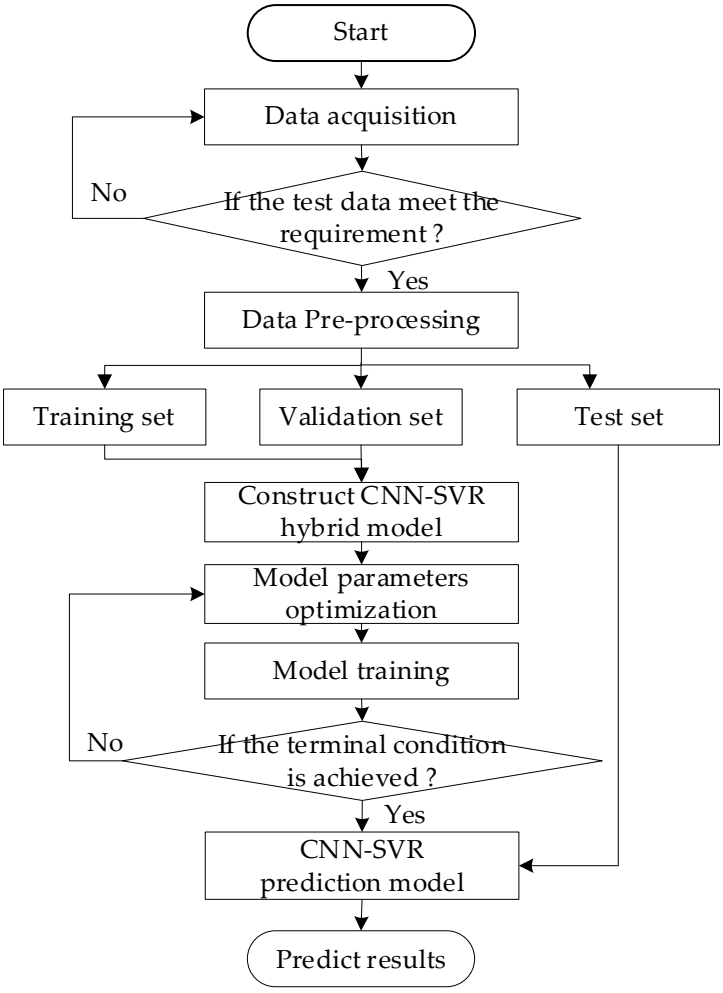


Figure 5. Flowchart for SRN prediction based on CNN–SVR.

3. Predictive Modeling and SRN Prediction

3.1. Experimental Design

The paper adopts an orthogonal experimental design method to develop the experimental program and collect the sample data needed to construct the road noise prediction model. The dynamic stiffness of the large front swing arm bushing, the dynamic stiffness of the small front swing arm bushing, the dynamic stiffness of the front and rear shock

absorber upper mounting bushings, the front and rear shock absorber damping force, and rear axle bushing dynamic stiffness, which have a large impact on the road noise, are selected as the design variables. Three level values of base level and 15% floating above (below) the base level are set for each variable, and an orthogonal test design is used to generate 27 groups of data samples.

Noise and vibration data are collected through actual vehicle road tests. The 24-channel LMS SCADAS Mobile data acquisition system from LMS Belgium and the Signature Testing-Advanced module of LMS Test.Lab18 are used to collect data online and analyze the data. Noise signals are collected using the non-directional BSWA sound pressure sensor, and vibration signals are collected using the PCB three-way vibration sensor. The sampling time is set to 10 s, the sampling frequency is set to 12,800 Hz, and the frequency resolution is 1 Hz. A three-way vibration acceleration sensor is arranged at the knuckle position of each tire, as well as at the body side and suspension side of the suspension-body attachment point. The sound pressure sensor is placed at the driver's right-ear position inside the vehicle. The driver's right ear is chosen as the measurement point mainly because there is relatively more space on the driver's right side, which can better reflect the noise situation in the vehicle, and it is easy to operate and measure. Some examples of sensor arrangement at test points are shown in Figure 6.

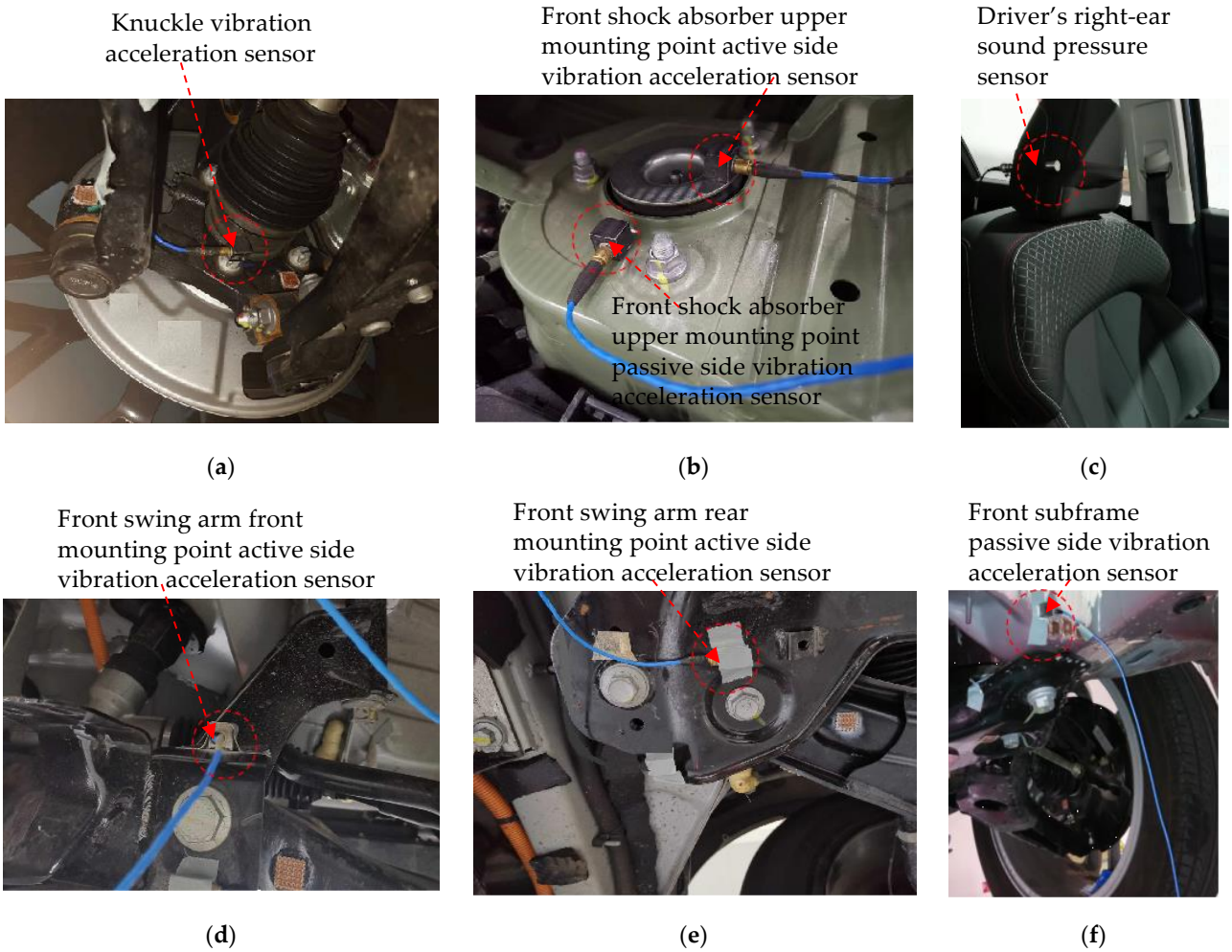


Figure 6. Sensor arrangement: (**a**) Knuckle vibration acceleration sensor; (**b**) Front shock absorber upper mounting point active side and passive side vibration acceleration sensor; (**c**) Driver's right-ear sound pressure sensor; (**d**) Front swing arm front mounting point active side vibration acceleration sensor; (**e**) Front swing arm rear mounting point active side vibration acceleration sensor; (**f**) Front subframe passive side vibration acceleration sensor.

It is important to choose a suitable working condition for the test. When the vehicle speed of electric vehicles is lower than 40 km/h, the motor and fan noise play a major role. When the vehicle speed is more than 80 km/h, the wind noise gradually becomes the dominant noise. When the vehicle is traveling at a medium speed of 40~80 km/h (especially on the rough road), vehicle suspension structure-borne noise makes up the majority of the interior noise. In order to better imitate the suspension structure-borne noise of the test vehicle, this paper chooses the constant speed of 60 km/h, and the rough asphalt pavement is used as the test road [37,38]. The reasons for choosing the rough asphalt road for road noise test mainly include the following two points: first, the rough road can fully stimulate the vehicle structure-borne noise and minimize the contribution of other noises; and second, the rough asphalt road is a typical road for passenger cars driving in urban roads, and the test results on this road can better reflect the road noise level of the vehicle under the actual driving road. The rough asphalt road used for the test is shown in Figure 7. During the test, external noise interference should be minimized by closing the windows, air conditioning, etc., and ensuring that no abnormal noise is generated. In addition to the driver, the necessary test personnel and test equipment should be used as far as possible to keep the vehicle in an unloaded state.



Figure 7. The rough asphalt road used for the test.

The measurements are performed at least three times to guarantee the accuracy of the data, and the difference in sound pressure levels between the three successive measurements is not allowed to exceed 0.5 dB(A). The sound pressure signal of the acoustic pressure sensor and the vibration signal of the acceleration sensor are finally measured. In this paper, road, tires, and vehicle speed are used as control variables. Tires of the same specification and pressure are selected, and the test is carried out on the same road at the same speed for sample collection. The knuckle vibration excitation is used as the input excitation to the suspension, and the focus is on the influence of the critical parameters, such as the dynamic stiffness of the chassis bushings and the shock absorber damping force on the road noise, to reduce the complexity of the model.

3.2. Methods and Investigated Vehicles

Through the above experimental tests, 27 groups of data samples that meet the requirements are collected. As a typical deep learning method, CNN requires a high amount of sample data, and in order to increase the sample size, we simultaneously collected data from 14 other similar benchmark vehicles from different manufacturers with the same suspension form. The selection criteria for these 14 vehicles remain the same as the previous

one vehicle, all based on the same suspension form, i.e., front McPherson suspension and rear torsion beam suspension, with the vehicles coming from different manufacturers and benchmark vehicles with similar price ranges and similar target customer groups in the market are selected, with brands including Chang'an Automobile, BYD Automobile, Geely Automobile, Chery Automobile, and other automobile brands. This approach can more comprehensively reflect the noise performance of this type of suspension form on different vehicles, thus increasing the diversity and universality of the data. In the data collection process, we used the same methods and equipment as before. Each vehicle is rigorously tested and calibrated to ensure it is in top condition. A total of 405 groups of data samples were obtained from 15 cars. The samples are normalized by [0, 1] to remove the impact of various data outlines and avoid masking the data that significantly affects the dependent variable. Equation (4) provides the data normalization formula [39].

$$x^* = \frac{x_0 - x_{\min}}{x_{\max} - x_{\min}} \tag{4}$$

where: $x_{\max}$ and $x_{\min}$ denote the maximum and minimum values in the dataset, respectively, and x_0 and x^* denote the value prior to and following normalization, respectively.

3.3. SRN Prediction Based on CNN–SVR

The SRN prediction model is constructed based on the proposed CNN–SVR method and multi-level decomposition architecture. For the first-level target of the driver's right-ear SPL in the vehicle, the integrated total value of 1/3 octave center frequency point of the noise spectrum in the frequency range from 20 Hz to 300 Hz is selected as the target to improve the computational efficiency, and the corresponding passive side vibration of the body at the second level is taken as the input. When constructing the second-level model, the vibration response of the passive side of the body is taken as the target, and the vibration of the active side of the suspension and the parameters of the elastic element are taken as inputs. When constructing the third-level model, the vibration response of the active side of the suspension is taken as the target, and the vibration excitation of the knuckle and the ball-hinge bushing dynamics parameters are taken as inputs.

For the adjacent layers in the multi-level decomposition architecture, this paper builds a 6-layer CNN–SVR hybrid model, which contains an input layer, two convolutional layers, a pooling layer, a fully connected layer, and an SVR regression output layer. The size of the convolutional kernel in the convolutional layer is 3×3 with a step size of 1, and the activation function is ReLU; the pooling layer, with a dimension of 2×2 and a step size of 2, employs the maximum pooling method; the last layer is the SVR regression output layer based on the Gaussian radial basis kernel function. Grid search is utilized for the model parameter optimization [40], the initial learning rate is 0.001, the training minimum batch size is 4, the total number of iterations is 400 epochs, and the optimization algorithm Stochastic Gradient Descent with Momentum (SGDM) is used.

In this paper, the Mean Square Error (*MSE*) and the coefficient of determination (R^2) are used as the criteria for evaluating the accuracy of the prediction model. The formulas for calculating the *MSE* and R^2 are denoted as Equations (5) and (6) [41,42], respectively:

$$MSE = \frac{1}{N}\sum_{i=1}^{N}(y_i - \widetilde{y}_i)^2 \tag{5}$$

$$R^2 = 1 - \frac{\sum_{i=1}^{N}(y_i - \widetilde{y}_i)^2}{\sum_{i=1}^{N}(y_i - \overline{y}_i)^2} \tag{6}$$

where: y_i denotes the real-vehicle test value for each sample response target; $\overline{y}_i$ represents the mean value of y_i; $\widetilde{y}_i$ is the model predicted value; and N is the total amount of samples.

Then, 6 of the aforementioned 405 sound samples are randomly selected as the test set, 319 samples are randomly selected as the training set, 80 samples are used as the validation set, and the model is trained based on the aforementioned parameters. The experiments are implemented using MATLAB 2022a on a workstation with an Intel(R) i9-12,900 K CPU and 64 GB of memory. Figure 8 displays the change of *MSE* expressed in Equation (5). In order to demonstrate the prediction effect of the proposed CNN–SVR hybrid model, this paper, based on keeping the original network parameters unchanged, also gives the prediction results of the traditional CNN model that is not combined with the SVR regression algorithm, and the traditional SVR model as a comparison. Table 1 exhibits the *MSE* and R^2 of the road noise prediction model on the validation set. From Figure 8 and Table 1, it can be obtained that with the increase of epochs, the *MSE* of the training set and validation set of the CNN–SVR hybrid model gradually decreases, and the model converges after 400 epochs. On the validation set, the R^2 of the proposed hybrid CNN–SVR model is 0.972, and *MSE* is 0.112, and its prediction accuracy surpasses both the traditional CNN and SVR models.

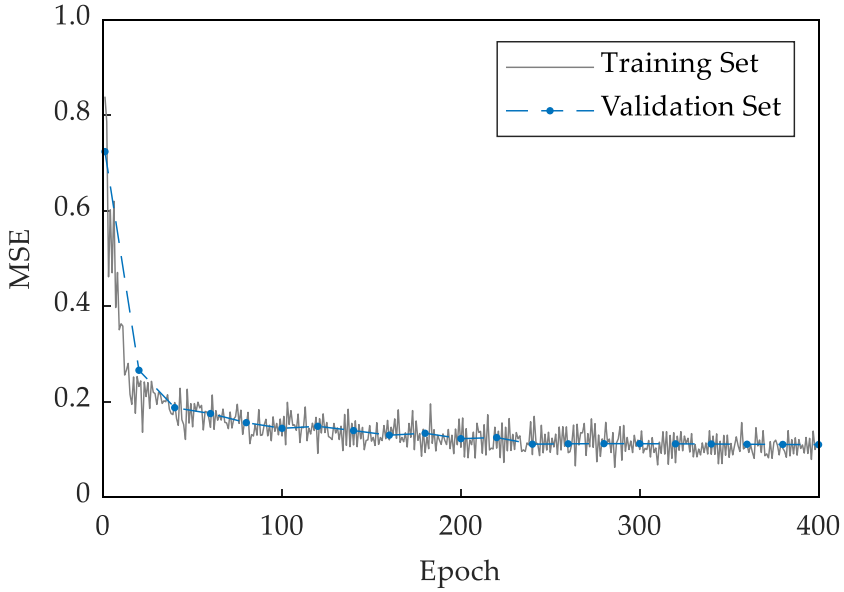


Figure 8. The training process of CNN–SVR hybrid model for road noise.

Table 1. *MSE* and R^2 of the model on the validation set.

Model	SPL at Driver's Right-Ear	
	MSE	R^2
SVR	0.457	0.873
CNN	0.286	0.915
SVR–CNN	0.112	0.972

To verify the effectiveness and generalizability of the CNN–SVR hybrid model more thoroughly, the test set of 6 groups of sound samples is analyzed. The model prediction results and the actual vehicle measurement outcomes, along with their respective errors, are compared in Figure 9. From Figure 9, it is noticeably observed that the CNN–SVR hybrid model has better accuracy in predicting as its maximum relative error is less than 2%, which is also lower than the other two models. Consequently, the CNN–SVR hybrid model is more favorable for future optimization and control of structural-borne vehicle noise.

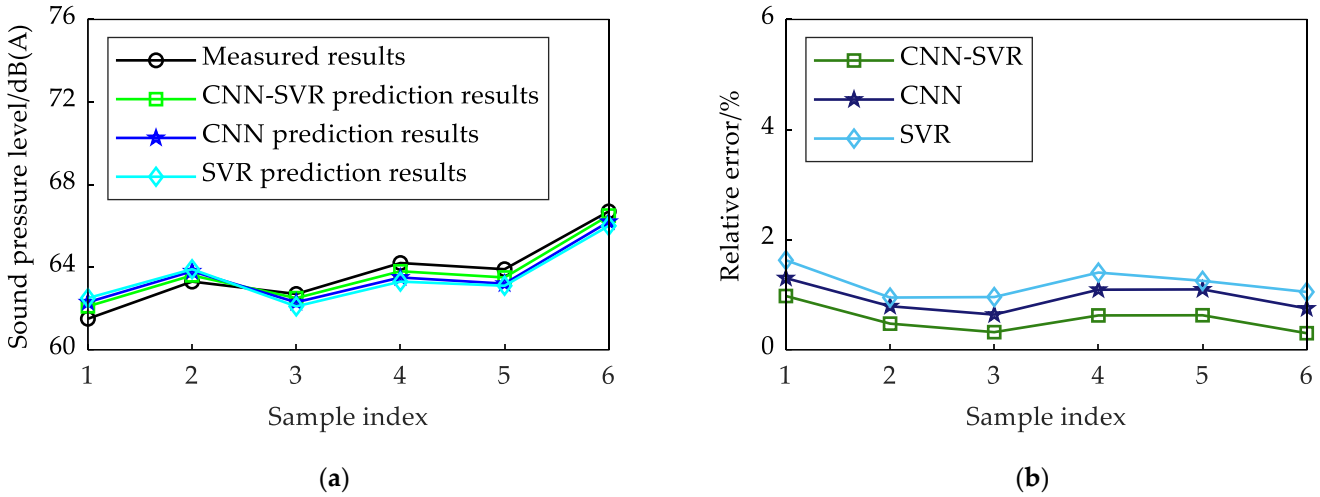


Figure 9. Comparison of measured and model-predicted results, as well as the relative errors between them: (**a**) Comparison of the outcomes; (**b**) Relative errors.

4. SRN Improving and Validation

Based on the road noise multi-level decomposition method and CNN–SVR hybrid model, the SRN of a vehicle to be improved is optimized. In engineering practice, extensive modification of chassis parameters is costly and time-consuming, and it is often the most cost-effective method to realize road noise performance improvement by modifying sensitive parameters on the critical path. This paper first performs a road noise sensitivity analysis using the CNN–SVR hybrid model in conjunction with the Mean Impact Value (MIV) algorithm [43]. Designable parameters, such as the dynamic stiffness of the chassis bushing and the damping force of the shock absorber, are perturbed within a specific range (±10%), and the impact of these perturbations on road noise is calculated. The goal is to identify the highly sensitive parameters and improve the optimization efficiency. The results of the sensitivity analysis are shown in Table 2, from which it can be seen that the rear axle bushing and the front swing arm bushing are highly sensitive factors affecting the interior noise.

Table 2. Sensitivity analysis results based on MIV.

Factors	MIV
Dynamic stiffness of rear axle bushing hollow-direction	0.495
Dynamic stiffness of the large front swing arm bushing hollow-direction	0.449
Dynamic stiffness of rear axle bushing solid-direction	0.396
Dynamic stiffness of the large front swing arm bushing solid-direction	0.375
Dynamic stiffness of the front shock absorber upper mounting bushing axle-direction	0.204
Dynamic stiffness of the rear shock absorber upper mounting bushing axle-direction	0.195
Rear shock absorber damping force	0.168
Front shock absorber damping force	0.159
Dynamic stiffness of the large front swing arm bushing axle-direction	0.123
Dynamic stiffness of the front shock absorber upper mounting bushing radial-direction	0.096
Dynamic stiffness of the rear shock absorber upper mounting bushing radial-direction	0.078
Dynamic stiffness of rear axle bushing axle-direction	0.063
Dynamic stiffness of the small front swing arm bushing radial-direction	0.057
Dynamic stiffness of the small front swing arm bushing axle-direction	0.036

Considering the cost, the difficulty of project implementation, and the impact on other properties such as maneuvering stability, smoothness, etc., the dynamic stiffness of rear axle bushing hollow-direction and solid-direction, as well as the dynamic stiffness of the large front swing arm bushing hollow-direction and solid-direction are regarded as design

variables, and the design space is the range of ±15% of the initial value of the design variable, and the amplitude of the driver's right-ear SPL is taken as the optimization target. Based on the decomposition structure in Figure 3, the numerical model for the prediction and optimization of SNR is established as Equation (7) [44]:

$$\begin{aligned} &\min y_k^{[p]} = f_k^{[p]}(x_1^{[p+1]}, x_2^{[p+1]}, \cdots x_d^{[p+1]}), \\ &p = 1, 2, \cdots, \ P_0 \quad k = 1, 2, \cdots, K \\ &s.t. \begin{cases} g_r^{[p]}(x^{[p]}) \le 0, \ \ r = 1, 2, \cdots, R \\ h_j^{[p]}(x^{[p]}) = 0, \ \ j = 1, 2, \cdots, J \\ x_d^{[p+1]} \in X_d^{[p+1]}, \ \ d = 1, 2, \cdots, D \end{cases} \end{aligned} \tag{7}$$

where: p denotes the proposed computational level in the hierarchical decomposition architecture; p_0 is the total level; $y_k^{[p]}$ is the optimization goals of the neighboring upper level; K is the number of optimization objectives in that level; $x_d^{[p+1]}$ is the adjacent lower level's design variables; D is the number of design variables in that level; $f_k^{[p]}$ is the nonlinear mapping function that maps the design variables to the optimization objective; $g_r^{[p]}(x^{[p]})$ denotes the inequality constraint function; $h_j^{[p]}(x^{[p]})$ is the equation constraint function; $x_d^{[p+1]}$ is the design variables of the $(p+1)$ level; and $X_d^{[p+1]}$ is the feasible domain of the dth design variable at the $(p+1)$ level. The constraints contain two items: One is that the driver's right-ear SPL should be lower than the initial value. The other is that the design variables' value range should be located within the feasible domain to guarantee feasibility in practical engineering applications.

Combined with the Genetic Algorithm (GA) to solve the optimal solution of the design variables, GA is a probabilistic optimization method that combines the genetics of nature and computer science, which is based on the principle of biological evolution, following the idea of "survival of the fittest" in biology [45], and its benefits include excellent adaptability, stability, quick convergence, and more [46]. The parameters of the GA are set as follows: population size is 100, crossover probability is 0.6, mutation probability is 0.01, and the maximum number of hereditary generations is 300. Table 3 displays the dynamic stiffness parameters of the chassis bushings (100 Hz) before and after optimization. Based on the optimization results, the bushing prototype is installed in the actual vehicle for validation. Table 4 compares the results of the model prediction with the measured results pre- and post-improvement. Figure 10 presents a comparison of noise spectra at the driver's right ear before and after improvement.

Table 3. Dynamic stiffness parameters of bushing.

Dynamic Stiffness of Bushings (100 Hz)	Original Value /(N·mm^{-1})	Optimized Value /(N·mm^{-1})
Rear axle bushing hollow-direction	1080	920
Rear axle bushing solid-direction	1969	1679
The large front swing arm bushing hollow-direction	883	761
The large front swing arm bushing solid-direction	2172	1873

Table 4. Model prediction outcomes and measured outcomes.

Status	Model Prediction Results /dB(A)	Measured Results /dB(A)	Relative Error /%
Pre-improvement	63.2	63.9	1.10
Post-improvement	60.8	61.3	0.82

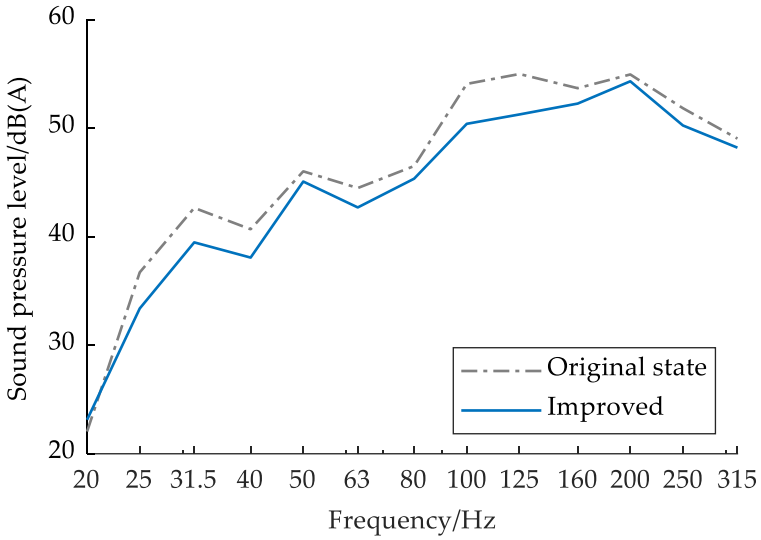


Figure 10. Comparison of noise spectra at the driver's right ear.

As shown in Table 4 and Figure 10, the SPL at the driver's right ear is 61.3 dB(A) after the improvement, which is 2.6 dB(A) lower than that before the improvement, with an improvement of 4.07%. The relative errors of model prediction results and measured results before and after the improvement are 1.10% and 0.82%, respectively, which are both less than 2%, verifying the accuracy and effectiveness of the proposed method.

5. Conclusions

This paper is focused on the prediction, analysis, and amelioration of automotive SRN. Primarily, adopting a viewpoint grounded in the transmission relationship of SRN and hierarchical target decomposition, we propose a multi-level target decomposition method for vehicle SRN. This method systematically dissects the entire vehicle road noise, layer by layer, through the chassis parts along the vibration transmission path. Subsequently, a thorough analysis is conducted, supplanting the need for a physical model of the vehicle. Subsequent to this, building upon the multi-level target decomposition framework, we introduce a road noise prediction method utilizing a CNN–SVR hybrid model, subsequently validating its efficacy on an actual vehicle. The R^2 for the proposed CNN–SVR hybrid model exceeds 0.97, while the *MSE* is lower than 0.2, thus establishing a prediction accuracy superior to that of both the traditional CNN model and SVR model. This validation underscores the efficacy and superiority of the proposed methodology. Finally, leveraging the established CNN–SVR hybrid model, a road noise sensitivity analysis is conducted on the vehicle earmarked for improvement. This analysis facilitates the identification of highly sensitive parameters influencing road noise, followed by optimization efforts targeting these parameters. The post-optimization measured results reveal a notable improvement of 4.07% in the driver's right-ear SPL as compared to the original state.

Author Contributions: All of the authors extensively contributed to the work. Conceptualization, X.J., L.Z. and J.P.; methodology, X.J. and L.Z.; software, X.J.; validation, X.J., L.Z. and H.H.; formal analysis, X.J.; investigation, X.J.; writing—original draft preparation, X.J.; writing—review and editing, L.Z. and H.H.; supervision, L.Y.; funding acquisition, J.P. All authors have read and agreed to the published version of the manuscript.

Funding: This research was funded by the National Key Research and Development Program of China: 2022YFB2503300; The open fund of State Key Laboratory of Vehicle NVH and Safety Technology: NVHSKL-202014, NVHSKL-202203; The independent project of State Key Laboratory of Vehicle NVH and Safety Technology: NVHSKL-ZS-202003.

Data Availability Statement: The authors do not have permission to share data.

Conflicts of Interest: Authors Xiaoli Jia, Jian Pang and Liang Yang were employed by the company Chongqing ChangAn Automobile Co., Ltd. The remaining authors declare that the research was conducted in the absence of any commercial or financial relationships that could be construed as a potential conflict of interest.

References

1. Parekh, D.; Poddar, N.; Rajpurkar, A.; Chahal, M.; Kumar, N.; Joshi, G.P.; Cho, W. A review on autonomous vehicles: Progress, methods and challenges. *Electronics* **2022**, *11*, 2162. [CrossRef]
2. Qin, Y.C.; Tang, X.L.; Jia, T.; Duan, Z.W.; Zhang, J.M.; Li, Y.N.; Zheng, L. Noise and vibration suppression in hybrid electric vehicles: State of the art and challenges. *Renew. Sustain. Energ. Rev.* **2020**, *124*, 109782. [CrossRef]
3. Shi, R.W.; Yang, S.C.; Chen, Y.Y.; Wang, R.; Zhang, M.Y.; Lu, J.Y.; Cao, Y.J. CNN-Transformer for visual-tactile fusion applied in road recognition of autonomous vehicles. *Pattern Recognit. Lett.* **2023**, *166*, 200–208. [CrossRef]
4. Darwiche, M.; Mokhiamar, O. SVR approach for predicting vehicle velocity for comfortable ride while crossing speed humps. *Alex. Eng. J.* **2022**, *61*, 6119–6128. [CrossRef]
5. Sha, M.Z.; Boukerche, A. Performance evaluation of CNN-based pedestrian detectors for autonomous vehicles. *Ad Hoc Netw.* **2022**, *128*, 102784. [CrossRef]
6. Ye, S.; Zhang, J.; Xu, B.; Zhu, S.; Xiang, J.; Tang, H. Theoretical investigation of the contributions of the excitation forces to the vibration of an axial piston pump. *Mech. Syst. Signal Process.* **2019**, *129*, 201–217. [CrossRef]
7. Fan, D.L.; Dai, P.S.; Yang, M.L.; Jia, W.Y.; Jia, X.L.; Huang, H.B. Research on Maglev Vibration Isolation Technology for Vehicle Road Noise Control. *SAE Int.* **2022**, *6*, 233–245. [CrossRef]
8. Huang, H.B.; Huang, X.R.; Ding, W.P.; Yang, M.L.; Yu, X.Y.; Pang, J. Vehicle vibro-acoustical comfort optimization using a multi-objective interval analysis method. *Expert Syst. Appl.* **2023**, *213*, 119001. [CrossRef]
9. Gao, Y.; Lou, X.B.; Zhou, H.Q.; Dong, L.; Yang, M.J. Transfer path identification and optimization of tire cavity noise in vehicle. *Automot. Eng.* **2019**, *41*, 1215–1220.
10. Yu, X.Y.; Min, F.J.; Wen, W.; Zhao, L.F.; Liu, Y. Structural transfer path analysis of tire/road noise. *Automot. Eng.* **2013**, *35*, 1031–1034.
11. Kido, I.; Ueyama, S.; Hashioka, M.; Yamamoto, S.; Tsuchiyama, M.; Yamaoka, H. Tire and road input modeling for low-frequency road noise prediction. *SAE Int.* **2011**, *4*, 1277–1282. [CrossRef]
12. Chen, S.M.; Peng, D.Z.; Wang, D.F.; Liang, J. Structural-acoustic coupling and optimal experimental design for automotive interior low frequency noise. *J. Jilin Univ. (Eng. Technol. Ed.)* **2014**, *44*, 1550–1556.
13. Xing, Y.F.; Wang, Y.S.; Shi, L.; Guo, H.; Chen, H. Sound quality recognition using optimal wavelet-packet transform and artificial neural network methods. *Mech. Syst. Signal Process.* **2016**, *66*, 875–892. [CrossRef]
14. Liang, L.Y.; Chen, S.M.; Li, P.R. The evaluation of vehicle interior impact noise inducing by speed bumps based on multi-features combination and support vector machine. *Appl. Acoust.* **2020**, *163*, 107212. [CrossRef]
15. Fan, D.L.; Jia, W.Y.; Jia, X.L.; Ma, D.Z.; Li, S.; Zhang, J.; Yu, X.Y. A Vehicle Structural-Borne Road Noise Prediction Method. China Patent CN113886974A, 4 January 2022.
16. Almiron, J.O.; Bianciardi, F.; Corbeels, P.; Pieroni, N.; Kindt, P.; Desmet, W. Vehicle road noise prediction using component-based transfer path analysis from tire test-rig measurements on a rolling tire. *J. Sound Vib.* **2022**, *523*, 116694. [CrossRef]
17. Sun, Z.J.; Xue, L.; Xu, Y.M.; Wang, Z. Overview of deep learning. *Appl. Res. Comput.* **2012**, *29*, 2806–2810.
18. Pang, J. *Automobile Body Noise and Vibration Control*, 1st ed.; Machinery Industry Press: Beijing, China, 2015; pp. 1–38.
19. Mao, J.; Chen, Z.D.; Qiu, Y.; Zhou, C.S.; Zhang, Y.N.; Yao, Z.Q. Road noise sound quality development by time-domain transfer path analysis. *Appl. Acoust.* **2022**, *41*, 815–821.
20. Huang, H.B.; Lim, T.C.; Wu, J.H.; Ding, W.P.; Pang, J. Multitarget prediction and optimization of pure electric vehicle tire/road airborne noise sound quality based on a knowledge-and data-driven method. *Mech. Syst. Signal Process.* **2023**, *197*, 110361. [CrossRef]
21. Zhou, W.Y.; Wang, H.; Wan, Z.B. Ore image classification based on improved CNN. *Comput. Electr. Eng.* **2022**, *99*, 107819. [CrossRef]
22. Goncalves, C.B.; Souza, J.R.; Fernandes, H. CNN architecture optimization using bio-inspired algorithms for breast cancer detection in infrared images. *Comput. Biol. Med.* **2022**, *142*, 105205. [CrossRef]
23. Xu, W.T.; Zhang, X.; Yao, L.; Xue, W.L.; Wei, B. A multi-view CNN-based acoustic classification system for automatic animal species identification. *Ad Hoc Netw.* **2020**, *102*, 102115. [CrossRef]
24. Luo, J.Q.; Fang, H.S.; Shao, F.M.; Zhong, Y.; Hua, X. Multi-scale traffic vehicle detection based on faster R-CNN with NAS optimization and feature enrichment. *Def. Technol.* **2021**, *17*, 1542–1554. [CrossRef]
25. Chen, L.; Zheng, W. Research on Railway Dispatcher Fatigue Detection Method Based on Deep Learning with Multi-Feature Fusion. *Electronics* **2023**, *12*, 2303. [CrossRef]
26. Xiao, Z.M.; Song, K.Y.; Gupta, M.M. Development of a CNN edge detection model of noised X-ray images for enhanced performance of non-destructive testing. *Measurement* **2021**, *174*, 109012. [CrossRef]
27. Lu, S.Y.; Lu, Z.H.; Zhang, Y.D. Pathological brain detection based on AlexNet and transfer learning. *J. Comput. Sci.* **2019**, *30*, 41–47. [CrossRef]

28. Gan, J.Y.; Jiang, K.Y.; Tan, H.Y.; He, G.H. Facial beauty prediction based on lighted deep convolution neural network with feature extraction strengthened. *Chin. J. Electron.* **2020**, *29*, 312–321. [CrossRef]
29. Ren, S.Q.; He, K.M.; Girshick, R.; Sun, J. Faster R-CNN: Towards real-time object detection with region proposal networks. *IEEE Trans. Pattern Anal. Mach. Intell.* **2017**, *39*, 1137–1149. [CrossRef]
30. Huang, H.B.; Huang, X.R.; Ding, W.P.; Zhang, S.W.; Pang, J. Optimization of electric vehicle sound package based on LSTM with an adaptive learning rate forest and multiple-level multiple-object method. *Mech. Syst. Signal Process.* **2023**, *187*, 109932. [CrossRef]
31. Guo, L.; Fang, W.G.; Zhao, Q.H.; Wang, X. The hybrid PROPHET-SVR approach for forecasting product time series demand with seasonality. *Comput. Ind. Eng.* **2021**, *161*, 107598. [CrossRef]
32. Wu, W.C.; Zhang, M.H.; Zhao, L.; Dong, H.; Zhang, J.Y. CFD-DPM data-driven GWO-SVR for fast prediction of nitrate decomposition in blast furnaces with nozzle arrangement optimization. *Process Saf. Environ.* **2023**, *176*, 438–449. [CrossRef]
33. He, Y.; Xiao, Z.; Li, Y.F.; Wu, P.C.; Liu, D.J.; Du, J. An assembly quality prediction method for automotive instrument clusters using CNN-SVR. *China Mech. Eng.* **2022**, *33*, 825–833.
34. Huang, H.B.; Wu, J.H.; Lim, T.C.; Yang, M.L.; Ding, W.P. Pure electric vehicle nonstationary interior sound quality prediction based on deep CNNs with an adaptable learning rate tree. *Mech. Syst. Signal Process.* **2021**, *148*, 107170. [CrossRef]
35. Zhou, Z.H. *Machine Learing*, 1st ed.; Tsinghua University Press: Beijing, China, 2016; pp. 121–145.
36. Zhong, W.; Gu, F. A multi-level deep learning system for malware detection. *Expert Syst. Appl.* **2019**, *133*, 151–162. [CrossRef]
37. Huang, H.B.; Wu, J.H.; Huang, X.R.; Ding, W.P.; Yang, M.L. A novel interval analysis method to identify and reduce pure electric vehicle structure-borne noise. *J. Sound Vib.* **2020**, *475*, 115258. [CrossRef]
38. Song, X.D.; Wu, D.J.; Li, Q.; Botteldooren, D. Structure-borne low-frequency noise from multi-span bridges: A prediction method and spatial distribution. *J. Sound Vib.* **2016**, *367*, 114–128. [CrossRef]
39. Shantal, M.; Othman, Z.; Bakar, A.A. A Novel Approach for Data Feature Weighting Using Correlation Coefficients and Min–Max Normalization. *Symmetry* **2023**, *15*, 2185. [CrossRef]
40. Tong, Q.B.; Liu, Z.Y.; Lu, F.Y.; Feng, Z.W.; Wan, Q.Z. A New De-Noising Method Based on Enhanced Time-Frequency Manifold and Kurtosis-Wavelet Dictionary for Rolling Bearing Fault Vibration Signal. *Sensors* **2022**, *22*, 6108. [CrossRef]
41. Goodfellow, L.; Bengio, Y.; Courville, A. *Deep Learning*, 1st ed.; Posts & Telecom University Press: Beijing, China, 2017; pp. 63–99.
42. Küçükönder, H.; Boyaci, S.; Akyüz, A. A modeling study with an artificial neural network: Developing estimation models for the tomato plant leaf area. *Turk. J. Agric. For.* **2016**, *40*, 203–212. [CrossRef]
43. Liu, G.; Yang, C.L.; Liu, S.; Xiao, C.B.; Song, B. Feature selection method based on mutual information and support vector machine. *Int. J. Pattern Recogn. Artif. Intell.* **2021**, *35*, 210–215. [CrossRef]
44. Boyd, S.; Vandenberghe, L. *Convex Optimization*, 1st ed.; Tsinghua University Press: Beijing, China, 2013; pp. 497–593.
45. Zhu, Z.; Cai, Y.F.; Chen, L.; Xia, C.G.; Shi, D.h. A Study on Parameter Matching of Hydro-mechanical Transmission System Based on Genetic Algorithm. *Automot. Eng.* **2020**, *42*, 74–80.
46. Zheng, Y.N.; Luo, J.; Chen, J.B.; Chen, Z.Y.; Shang, P.P. Natural gas spot price prediction research under the background of Russia-Ukraine conflict-based on FS-GA-SVR hybrid model. *J. Environ. Manag.* **2023**, *344*, 118446. [CrossRef] [PubMed]

Disclaimer/Publisher's Note: The statements, opinions and data contained in all publications are solely those of the individual author(s) and contributor(s) and not of MDPI and/or the editor(s). MDPI and/or the editor(s) disclaim responsibility for any injury to people or property resulting from any ideas, methods, instructions or products referred to in the content.